AERODYNAMICS AND AEROACOUSTIC RESPONSE OF LOW-REYNOLDS NUMBER PROPELLERS WITH UNEQUAL BLADE SPACING

Dima Usov, Timos Chronis, and Antonio Filippone
Department of Mechanical and Aerospace Engineering, The University of Manchester
Manchester, United Kingdom

ABSTRACT

This study investigates the aerodynamic and aeroacoustic performance of a two-bladed, radially asymmetric propeller featuring 90-degree blade spacing under static flight conditions. This configuration was used to isolate the effect of blade spacing. Results were compared against a symmetric, reference propeller with equivalent blade geometry and similarity parameters. Performance tests showed aerodynamic efficiency parity, despite a slight reduction in both thrust and torque. Free-field acoustic measurements revealed a redistribution of tonal energy, with dominant tones shifting from the blade-passing frequency (BPF) to 0.5BPF. This shift moved acoustic energy into the frequency range with greater attenuation under A-weighting, resulting in reduced perceived loudness. While broadband noise was reduced in the mid-frequency domain, an increase was observed above 10 kHz. The results suggest that uneven blade spacing offers a perceptually effective noise mitigation strategy for UAS applications.

NOTATION

*

Symbols

A A-weighting function

c_0 Speed of sound, $\mathrm{m\,s^{-1}}$

C_P Time-averaged propeller power coefficient

C_{P_i} Induced power coefficient

$C_{P_{\text{meas}}}$ Measured power coefficient

C_T Time-averaged propeller thrust coefficient

d Observer distance, m

$\mathrm{d}C_l$ Spanwise lift coefficient

$\mathrm{d}C_t$ Spanwise thrust coefficient

D Propeller diameter, m

f Frequency, Hz

f_n Frequency at n-th BPF harmonic, Hz

f^+ Normalised frequency by the BPF, Hz

F_z Time-averaged propeller axial force, N

M Mach number

M_{tip} Blade-tip Mach number

n Angular speed, rps

p_0 Reference acoustic pressure, Pa

P Time-averaged propeller power, W

Q Time-averaged propeller torque, N m

R^2 Coefficient of determination

Re Reynolds number

t Time, s

T Time-averaged propeller thrust, N

W Sound power, W

W_0 Reference acoustic power, W

Δf Frequency resolution, Hz

ε Mean absolute percentage error

θ Observer angle, deg

ρ Air density, $\mathrm{kg\,m^{-3}}$

τ Facility time-scale, s

Ω Angular speed, rpm

Copyright Statement
The authors confirm that they, and/or their company or organization, hold copyright on all of the original material included in this paper. The authors also confirm that they have obtained permission, from the copyright holder of any third-party material included in this paper, to publish it as part of their paper. The authors confirm that they give permission, or have obtained permission from the copyright holder of this paper, for the publication and distribution of this paper as part of the ERF proceedings or as individual offprints from the proceedings and for inclusion in a freely accessible web-based repository.

*

Acronyms

AAM Advanced Air Mobility

BPF Blade-Passing Frequency

BVS Bluntness Vortex Shedding

CAA Civil Aviation Authority

eVTOL electric Vertical Take-Off and Landing

EASA European Aviation Safety Agency

FAA Federal Aviation Administration

FM Figure of Merit

ISA International Standard Atmosphere

LB Leading Blade

MAPE Mean Absolute Percentage Error

OASPL Overall Sound Pressure Level

OASPLA A-weighted Overall Sound Pressure Level

PSD Power Spectral Density

PWL Sound Power Level

PWM Pulse-Width Modulation

RPM Revolutions per Minute

SLA Stereolithography Apparatus

SPL Sound Pressure Level

SPLA A-weighted Sound Pressure Level

TB Trailing Blade

UAS Unmanned Aerial System

VP-R Reference propeller with 180-degree blade spacing

VP-9 Asymmetric propeller with 90-degree blade spacing

INTRODUCTION

The rapid expansion of Unmanned Aerial Systems (UAS) and the emerging Advanced Air Mobility (AAM) sector is reshaping modern aviation. Most UASs and electric Vertical Take-Off and Landing (eVTOL) aircraft in the civil sector rely on low-Reynolds-number rotary-wing devices – such as propellers or rotors – for both thrust and lift. These systems inherently generate acoustic emissions that can negatively impact public acceptance and regulatory compliance.

Psychoacoustic studies have highlighted that UAS noise is perceived as more annoying than other transportation noise sources (Ref. 1). This is primarily due to distinctive acoustic features, such as tonal and high-frequency broadband content. Torija et al. (Ref. 2) further showed that, while loudness diminishes with altitude, perceived annoyance declines less rapidly, emphasising that high-frequency components are a key factor in noise perception. These findings suggest that mission-based noise mitigation (e.g., operating at higher altitude) may not be sufficient, underscoring the need for design-level interventions.

Regulatory agencies, including the CAA (Ref. 3), FAA (Ref. 4), and EASA (Ref. 5), are developing certification frameworks for UAS and eVTOL noise, increasing pressure on manufacturers to adopt low-noise designs. In this context, modifying the acoustic characteristics of propellers is a critical enabler for sustainable urban air mobility.

Previous research has explored design-based noise reduction strategies, such as blade geometry optimisation (Refs. 6, 7) and tip speed control (Ref. 8). Another promising strategy is the introduction of uneven blade spacing, which alters the tonal distribution of propeller noise. Uneven blade spacing has been employed in systems such as Fenestron™ rotors and scissor-tail rotors, and even in single-bladed designs like the Everel propeller and Bölkow Bo-103 helicopter. A recent example includes an asymmetric propeller developed for a UAV platform, featuring two blades at an acute azimuth separation, with axial separation offset – an arrangement similar to *sycamore* seed morphology (Refs. 9, 10).

Studies from adjacent fields on radial and axial fans have consistently shown that uneven blade spacing can reduce tonal amplitudes at blade-passing frequency (BPF) harmonics while spreading energy to sub-harmonics (Refs. 11–13). This redistribution results in a more diffuse spectral profile, which is perceived as less annoying (Ref. 11). Notably, the overall unweighted Sound Pressure Level (SPL) and performance remained largely unchanged (Refs. 13, 14).

Similar findings have been reported in propeller and rotor studies. Shahady et al. (Ref. 15) and Chirico et al. (Ref. 16) demonstrated that small changes in blade spacing produced significant tonal redistribution, sometimes at the cost of slight increases in unweighted SPL. Other studies, such as those by Dobrzynski (Ref. 17), have found that optimally spaced blades could reduce A-weighted SPL by up to 4 dB due to frequency shifting. Aerodynamic penalties, when observed, were generally minimal.

However, most prior studies have focused on systems with four or more blades, where aerodynamic interference between blade pairs can influence the acoustic signature. This raises a critical question: How does the blade spacing angle in isolation contribute to the redistribution of acoustic spectra?

A previous study by the authors (Ref. 18) examined the aerodynamic and acoustic response of propellers with unequal blade spacing angles manufactured using a Stereolithography Apparatus (SLA). The results indicated that 90-degree blade spacing offered a favourable trade-off between tonal and broadband noise. However, inconsistencies introduced by the manual post-processing of prototypes may have affected the observed acoustic characteristics.

The current study builds on this prior work by using bespoke, radially *asymmetric* two-bladed propellers with a 90-degree spacing between the leading and trailing blades, manufactured by a specialist company to ensure improved surface quality and geometric fidelity. An experimental campaign was conducted to characterise both the aerodynamic performance and aeroacoustic response of the asymmetric design in static conditions. The results are directly compared with a conventional symmetric propeller of equivalent blade geometry and similarity parameters. By isolating the blade spacing angle – free from aerodynamic interference effects between blade pairs – the study enables a clearer assessment of how blade spacing angle alone influences acoustic energy spectral distribution. The overarching goal is to inform the design of quieter UAS propellers by targeting specific acoustic features through simple geometric interventions.

METHODS

Propeller geometry

A set of two 16×5.5 inch propellers was considered in this study, shown in Fig. 1, an asymmetric propeller that featured a 90-degree blade spacing, VP-9, and a conventional off-the-shelf propeller, VP-R, with equivalent blade geometry and similarity parameters. The asymmetric propeller's spacing was chosen based on the preliminary findings by the authors (Ref. 18). The asymmetric propeller's hub was designed to eliminate mass eccentricity inherited from a non-uniform distribution of blades around the axis of rotation. A set of outdoor flight tests was conducted using a wingless multirotor unmanned aerial system to assess the structural integrity of these lifting propellers (Ref. 19).

(a) Conventional propeller, VP-R, with 180-degree blade spacing

(b) Asymmetric propeller, VP-9, with 180-degree blade spacing

Figure 1: Set of 16×5.5 inch propellers.

Static performance measurements

Static performance measurements were conducted by the propeller manufacturer. The test procedures and results were documented in a performance report, which was provided upon delivery of the propellers. Propellers were mounted on the test rig in a puller configuration, and time-averaged thrust and torque values were recorded across a range of angular velocities up to 7,000 rpm.

The static aerodynamic response of the propellers was assessed using an angular speed ramping procedure, divided into ten evenly spaced Pulse-Width Modulation (PWM) signal steps. This process was automated to ensure repeatability. Each PWM step was held for 6 seconds, during which thrust and torque were measured. Time-averaged performance data were extracted from a steady-state time window, excluding the first 2 seconds and the final second of each step to minimise the influence of transient effects caused by propeller inertia.

All six VP-9 propeller assemblies were tested, with each propeller measured twice, resulting in a total of 12 test runs. During testing, ambient conditions were recorded as follows: air temperature of 25.2 °C, atmospheric pressure of 990 hPa, and air density of 1.159 $\mathrm{kg\,m^{-3}}$.

These measurements were later independently verified by members of the author team at the deHavilland Low Speed Wind Tunnel at the University of Glasgow under no-wind conditions as part of an axial-flight performance characterisation campaign for V-series propellers. This experimental campaign forms part of ongoing work on asymmetric propeller characterisation, which is yet to be published.

Free-field acoustic measurements

Free-field acoustic measurements were conducted in an anechoic chamber at the University of Salford, following a setup similar to that described in (Ref. 20). A photograph showing the instrumentation within the chamber is presented in Fig. 2. The chamber had working dimensions of $5.4 \times 4.1 \times 3.3$ meters, a cut-off frequency of 50 Hz, and a specified background sound pressure level of -12.4 dBA.

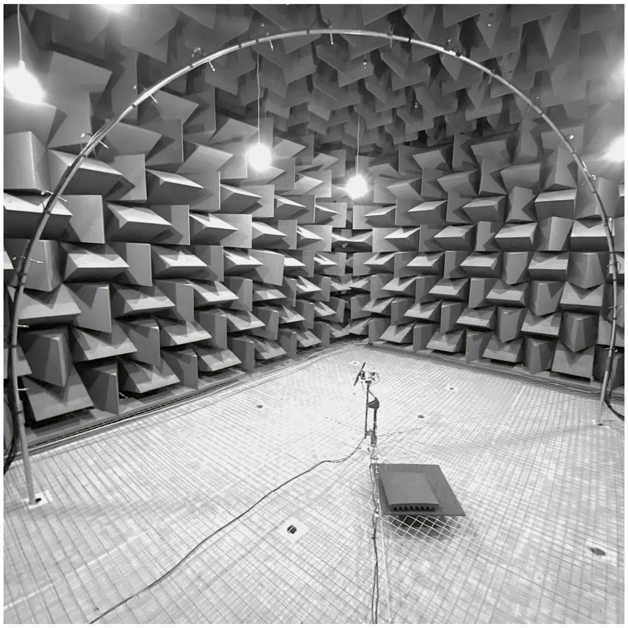

Figure 2: Anechoic chamber instrumentation and setup.

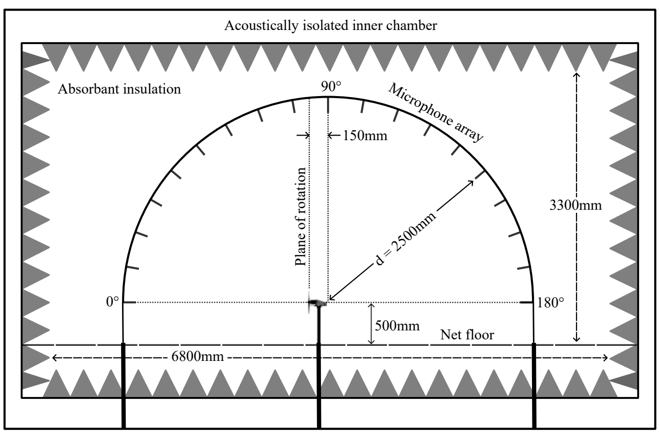

Figure 3: Anechoic chamber schematics.

A microphone array comprising nineteen 1/2-inch pressure microphones – nine Brüel and Kjær 4963 and nine GRAS 46AO – was arranged along a 2.5-meter arc positioned diagonally within the chamber. The microphones were uniformly spaced at 10-degree intervals across observation angles θ ranging from 0 to 180 degrees. The propeller test rig was placed at the centre of the chamber, such that the rotational plane of the propeller was orthogonal to the arc's plane. The propeller hub was concentrically aligned with the arc centre, with a small offset of 150 mm towards the microphone at 0 degrees, as shown in Fig.3. The microphone at 180 degrees was located within the propeller wake. All microphones were set to sample at a rate of 50 kHz. Standard International Atmosphere (ISA) conditions at sea level were assumed for all atmospheric data.

The propellers were installed in a tractor configuration on a static rig. The rig included a brushless MN505-S direct-current electric motor, an AT115 electronic speed controller, and an optical tachometer. Tachometer signals were recorded at 50 kHz via a data acquisition system. Motor speed was controlled using a PWM signal generated on an 8-bit micro-controller. This yielded a PWM resolution limit of 7.8 µs, corresponding to approximately 7 rpm steps.

The test matrix is summarised in Table 1. Each test point was repeated three times. The reported measured RPM values represent the average across these runs. The absolute percentage error between target and measured RPM remained below 0.5% for all test points. Although thrust was not measured directly, it was inferred from experimental performance curves corresponding to the specified angular speed.

Table 1: Test matrix.

	Test	Ω^a [rpm]	Ω'^b [rpm]	$\Delta\Omega^c$ [%]	τ^d [s]
VP-R	1	5,000	5,002	0.04	80
	2	4,500	4,507	0.16	89
	3	4,000	4,005	0.13	101
	4	3,500	3,498	0.06	117
VP-9	5	5,000	5,012	0.24	82
	6	4,500	4,521	0.46	91
	7	4,000	4,018	0.45	104
	8	3,500	3,510	0.29	120

^{a}target RPM; ^{b}measured RPM; ^{c}absolute percentage error with respect to the target RPM; ^{d}facility time-scale.

Due to the enclosed nature of the anechoic facility, the potential onset of recirculation and the associated risk of acoustic contamination were anticipated. The ingestion of higher-energy flow contributes to increased unsteady pressure loading along the blade, which in turn affects both performance metrics and acoustic measurements (Ref. 21). At an operating speed of 5,000 rpm, the facility time-scale (Ref. 22) was estimated to be 80 seconds for the VP-R and 82 seconds for the VP-9 propellers. Figure 4 illustrates the susceptibility of the acoustic response to recirculation onset. As shown, the Sound Power Level (PWL) spectrum following the presumed onset of recirculation – depicted by the red line – exhibits elevated energy content at specific harmonics, consistent with findings in (Refs. 23–26). This observation corroborates the importance of carefully timing the measurement window to mitigate data contamination. The precise time of recirculation onset remains undetermined, and a detailed characterisation of the chamber's recirculation behaviour under the current experimental setup lies beyond the scope of this study.

Therefore, a systematic test procedure was employed to minimise recirculation effects. Each test began with the propeller at rest, followed by the initiation of acoustic data recording, which was preset for 30 seconds. The propeller was then spun up, and data acquisition continued throughout the recording window. Upon completion, the propeller was brought to rest, allowing the flow to settle before the next test. In post-processing, the segment of data prior to reaching the target angular speed was excluded. The sound pressure signal was conservatively truncated to a 5-second time-segment starting after the propeller reached its target RPM to minimise the acoustic contamination associated with the onset of recirculation.

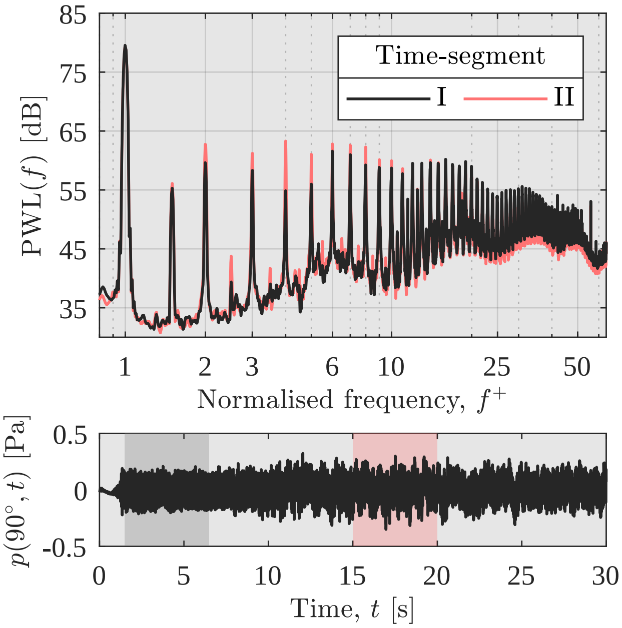

Figure 4: Flow recirculation effect on Sound Power Level.

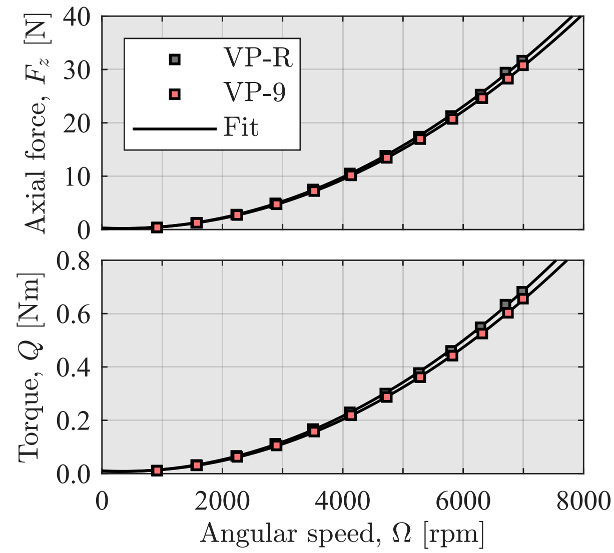

Figure 5: Time-averaged propeller thrust (top) and torque (bottom).

RESULTS

Aerodynamic response

The thrust and torque variations with RPM for both propellers are plotted in Fig. 5. A second-order polynomial curve was fitted to the two sets of data, indicated by the solid lines. The coefficients of determination for the fits were greater than $R^2 = 0.999$ in all cases. The thrust and power were nondimensionalised according to the propeller definitions of the coefficients:

$$C_T = \frac{F_z}{\rho n^2 D^4}, \tag{1}$$

$$C_P = \frac{P}{\rho n^3 D^5}, \tag{2}$$

$$P = 2\pi n Q, \tag{3}$$

where n is the angular speed in revolutions per second. The thrust coefficient is plotted in Fig.6. The difference between the two propellers is given in terms of the mean absolute percentage error (MAPE) metric and was found to be between 3% and 6%. This metric is defined as:

$$\varepsilon = \left| \frac{X_R - X_9}{X_R} \right| \times 100, \tag{4}$$

where X_R denotes values for the reference propeller and X_9 denotes values for the propeller with blade spacing of 90 degrees. The Reynolds number of the propellers at 75% of their radius varied from 20,000 to 200,000. The increase in thrust coefficient with RPM is related to the increase in the Reynolds number of the blade, as noted in previous works (Refs. 22, 27, 28). At low Reynolds numbers, the airfoil's lift coefficient decreases while its drag coefficient increases, leading to an overall lower thrust coefficient. An accompanying decrease in the power coefficient with RPM would be expected due to the same effect. However, the opposite variation was observed, as shown in Fig.7. An increase in lift slope and drag coefficient associated with compressibility effects also became a factor for RPMs higher than 5,000, at which speed the blade tips exceeded the limit of $M = 0.3$, causing pronounced increases in C_T and C_P at the higher end of the speed range.

To interpret the difference in aerodynamic performance between VP-R and VP-9, computations of the blade loads were performed using RORI, a solver based on potential flow theory. RORI incorporates the generalised dynamic wake model by Peters and He (Ref. 29) to calculate the induced flow velocities at the blades as a result of the generation of aerodynamic loads. This is coupled with blade-element theory for the computation of the loads themselves. More details of the RORI implementation are given in (Ref. 30). The results for the spanwise distributions of the thrust and lift coefficient are shown in Fig. 9 and Fig. 10 respectively. Compared to the reference case, the increase in downwash velocity experienced by the trailing blade (TB) of the VP-9 propeller due to its proximity to the leading blade (LB) causes a decrease in lift, and hence thrust. Conversely, the increase in thrust on the leading blade is smaller, leading to an overall reduction in thrust compared to the VP-9 propeller.

The thrust delivered by the reference propeller, VP-R, was higher than the thrust of the asymmetric propeller, VP-9. However, the power was also higher, leading overall to a similar efficiency, quantified in static conditions in terms of the

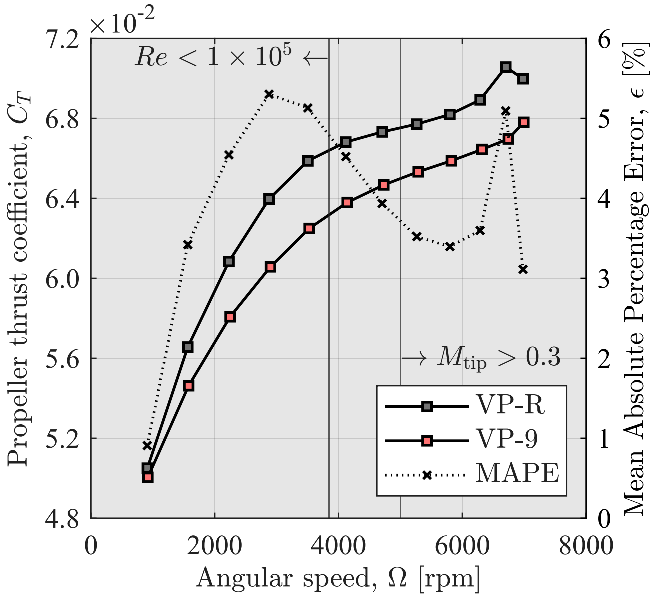

Figure 6: Time-averaged propeller thrust coefficient.

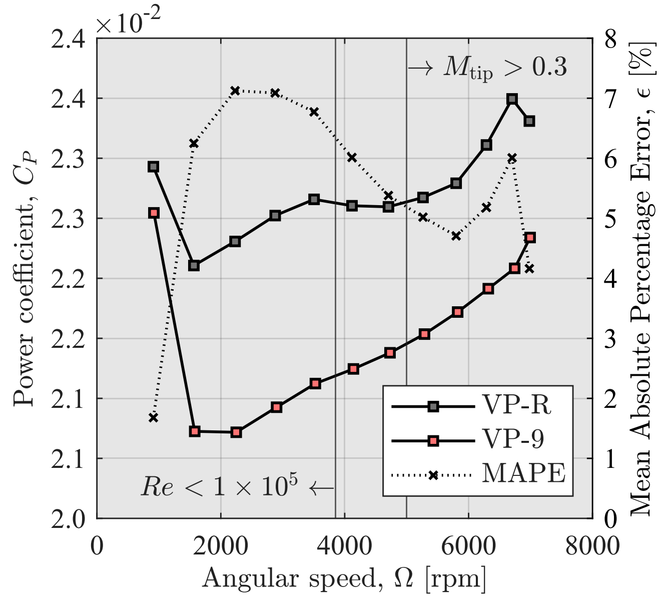

Figure 7: Time-averaged propeller power coefficient.

Figure of Merit (FM):

$$\mathrm{FM} = \frac{C_{P_i}}{C_{P_{\mathrm{meas}}}} = \frac{\sqrt{2C_T}^3}{2C_{P_{\mathrm{meas}}}}. \tag{5}$$

The variation of FM is plotted in Fig.8. The difference in FM between the two propellers is lower than 1% over the working range of RPM. This parity in aerodynamic efficiency between the two designs is in agreement with previous findings (Refs. 16, 17).

Aeroacoustic response

For the spectral analysis of the experimental data, a constant partition size of 2^{15} and a Hanning window of length 2^{14} with a 50% overlap were used, giving a frequency resolution of $\Delta f \approx 1.53$ Hz. The Power Spectral Density (PSD) was obtained using Welch's method (Ref. 31).

Sound Power Level The frequency response of the PWL in decibels was calculated using the equation from (Ref. 21), as follows:

$$W(f) = \frac{2\pi d^2}{\rho c_0} \int_0^\pi \mathrm{PSD}(\theta, f) \Delta f \sin(\theta)\, \mathrm{d}\theta, \tag{6}$$

$$\mathrm{PWL}(f) = 10 \log_{10} \left(\frac{W(f)}{W_0} \right) \tag{7}$$

where d is the distance from the source to the observer, which corresponds to the radius of the microphone arc array; ρ and c_0 are the ambient air density and speed of sound assumed from the standard atmosphere at sea level, respectively, and W_0 is the reference acoustic power assumed at 10^{-12} watts.

Figure 11 illustrates the measured frequency response of PWL at 5,000 rpm for observation angles ranging from 0 to 180 degrees, with spectral content shown from 50 Hz to 16 kHz. The black curve depicts the response of the reference propeller, while the red curve shows the response of the propeller with 90-degree blade spacing (VP-9). Vertical lines indicate frequencies corresponding to one-half, first, second, and third BPF harmonics, where one-half BPF corresponds to the shaft rotational frequency.

In the low-frequency domain, $f \in [50, 1{,}000]$ Hz, the PWL response of the VP-9 propeller demonstrated distinct tonal redistribution. Tones components at intermediate BPF harmonics (e.g. 0.5BPF, 1.5BPF, 2.5BPF, etc.) showed a pronounced increase, while most tones at principal harmonics (e.g. 1BPF, 2BPF, 3BPF, etc.) were generally either reduced or remained unchanged. Notably, the tone at 0.5BPF increased by approximately 30 dB, whereas the tone at 1BPF decreased by around 11 dB. The dominant amplification at 0.5BPF was consistent across the tested RPM range, while the frequency associated with maximum tonal reduction at other RPMs was 3BPF, as seen in Fig. 14. This pattern reflects a spectral redistribution – or "spreading" – of acoustic energy content, in agreement with findings from previous studies on fans and propellers with multiple blade-pairs (Refs. 11–13, 15–17). Moreover, the propeller broadband noise in the low-frequency domain was largely unaffected by uneven blade spacing, except for the region around 0.5BPF.

The reference VP-R propeller also exhibited a weak tonal content at intermediate BPF harmonics – an occurrence frequently observed in the experimental studies (Refs. 22, 32–36). This recurring phenomenon has been recently corroborated by Iannotta et al. (Ref. 37), who emphasised that it is an experimental artefact caused by slight geometric inconsistencies between propeller blades, likely introduced during the manufacturing process.

In the mid-frequency domain, $f \in (1{,}000, 10{,}000]$ Hz, all tonal peaks of the VP-9 propeller were reduced compared to those of the VP-R propeller, with reduction ranging from ap-

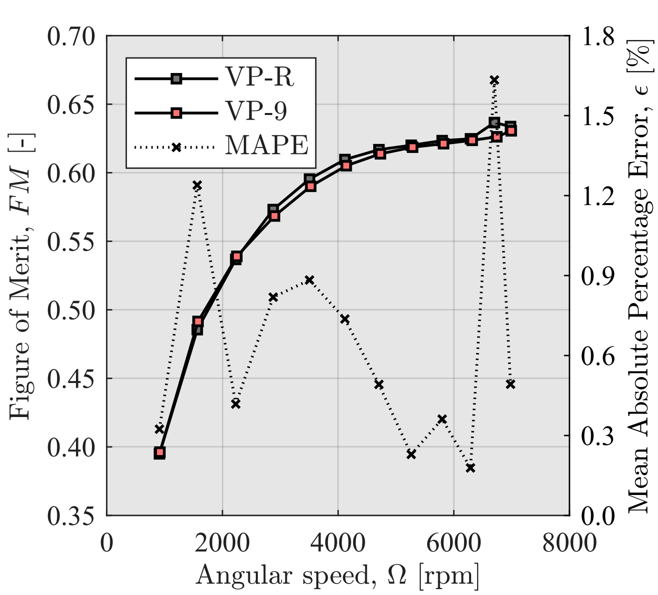

Figure 8: Figure of Merit.

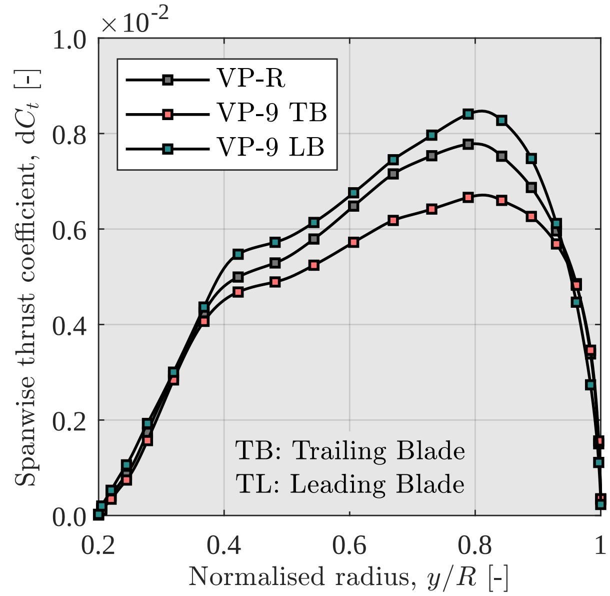

Figure 9: Spanwise distribution of blade thrust coefficient.

proximately 3 dB near the lower to 6 dB near the upper limit of the mid-frequency interval. The VP-9 propeller also exhibited consistently lower broadband noise across the mid-frequency interval, with the most pronounced reduction occurring at the higher frequencies of the band. Based on the spectral location, this broadband attenuation is likely associated with trailing-edge noise mechanisms.

However, the trailing blade of the VP-9 propeller operates within the intensified downwash due to its proximity to the trailed wake of the leading blade (Ref. 38). Thus, it perceives a more energetic inflow. This operating condition should augment the turbulence ingestion and associated effects on broadband noise. The observed broadband noise reduction, hence, suggests a more complex interaction between inflow turbulence and airfoil self-noise mechanisms. As highlighted by Botero-Bolivar et al. (Ref. 39), higher free-stream turbulence has been shown to lead to an increase in the trailing-edge noise source emitted by an airfoil through the phenomenon of turbulence penetration into the boundary layer, although the extent of this effect was also dependent on the relative length scales of the free-stream and the boundary layer turbulence. A subsequent investigation showed that the effect of inflow turbulence on the wall pressure spectrum near the trailing edge at frequencies higher than 1,000 Hz became more pronounced as the angle of attack was increased (Ref. 40). In the present case, the observed broadband noise reduction suggests that the reduction in effective angle of attack has a more significant effect on the airfoil self-noise than any increase in inflow turbulence, at least for frequencies below 10,000 Hz. Further investigation is still required to clarify this governing mechanism and fully understand the sources contributing to the noise reduction.

In the high-frequency domain, $f \in (10{,}000, 16{,}000]$ Hz, the VP-9 propeller showed an increase in broadband noise, which can be attributed to Bluntness Vortex Shedding (BVS) based on its spectral domain (Ref. 41).

Directivity The Overall Sound Pressure Level (OASPL) at a given emission angle was obtained by first calculating the frequency response of the SPL in decibels, followed by the linear summation of the SPL spectra over the frequency range from 50 Hz to 25 kHz, and converting it back to decibel scale.

$$\mathrm{SPL}(\theta, f) = 10\log_{10}\left(\frac{\mathrm{PSD}(\theta, f)\,\Delta f}{{p_0}^2}\right), \tag{8}$$

$$\mathrm{OASPL}(\theta) = 10\log_{10}\left(\int_{f_{\min}}^{f_{\max}} 10^{\mathrm{SPL}(\theta,f)/10}\mathrm{d}f\right), \tag{9}$$

where p_0 is reference acoustic pressure level, assumed at 20 µPa. Correction for human hearing perception was made by applying a standard A-weighting function, $A(f)$, as follows:

$$\mathrm{SPLA}(\theta, f) = 10\log_{10}\left(\frac{\mathrm{PSD}(\theta, f)\,\Delta f \cdot A(f)}{p_0^2}\right). \tag{10}$$

Directivity plots of the OASPL at 5,000 rpm are shown in Fig. 12. The VP-9 propeller demonstrated higher OASPL values at emission angles between 20 and 150 degrees, with a maximum increase of approximately 6 dB observed near the plane of rotation. This suggests an increase in the thickness noise of the VP-9 propellers, which is typically dominant in the plane of rotation. The OASPL of the VP-9 propeller was higher than that of the VP-R at all tested RPMs, except for certain emission angles at 4,500 rpm, as shown in Fig. 15 of the Appendix.

The A-weighted OASPL (OASPLA), shown in Fig. 13, reveals an opposite trend. The VP-9 propeller exhibited lower OASPLA values across the entire observation domain. The greatest reductions – around 3.4 dB – occurred at 0 and 180 degrees. In contrast to unweighted OASPL results, only a

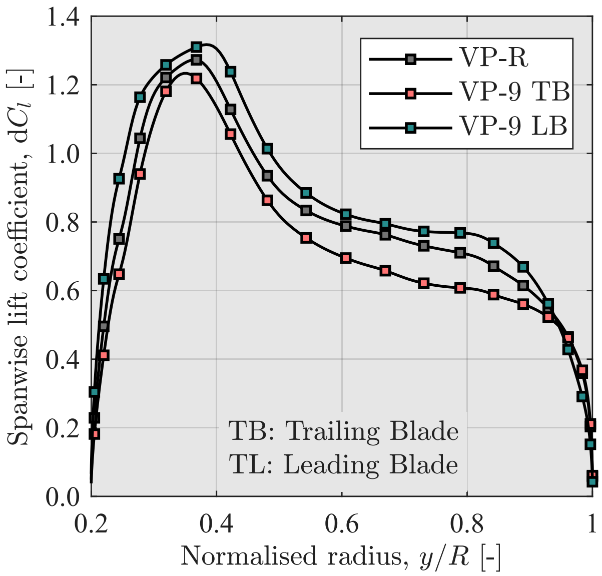

Figure 10: Spanwise distribution of blade lift coefficient.

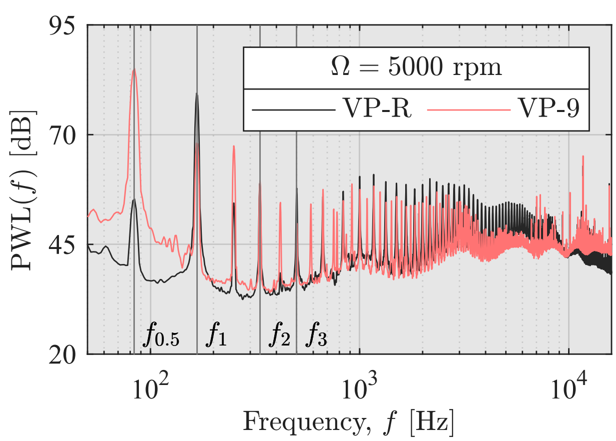

Figure 11: Sound Power Level.

marginal difference was observed at emission angles near the plane of rotation. This indicates that the spectral energy redistributed by the uneven blade spacing falls predominantly in frequency regions less perceptible to the human ear. The A-weighting attenuation of the VP-9 spectrum became less pronounced at lower RPMs, as seen in Fig. 16 of the Appendix.

These results indicate that the VP-9 propeller offers a more favourable acoustic signature for human hearing perception, despite an overall increase in radiated acoustic energy. This effect can be attributed to a redistribution of spectral energy. As shown in Fig.11, the dominant tonal component of the VP-9 shifted from 1BPF to 0.5BPF, effectively relocating acoustic energy into a frequency region where the A-weighting filter applies greater attenuation (Ref. 17). This spectral shift reduces perceived loudness, highlighting the potential of uneven blade spacing as an effective perceptual noise mitigation strategy for UAS applications. However, as outlined by Torija et al. (Ref. 2), loudness is not the primary factor driving perceived annoyance. Therefore, a comprehensive psychoacoustic evaluation is needed to determine whether these propellers exhibit reduced perceived annoyance.

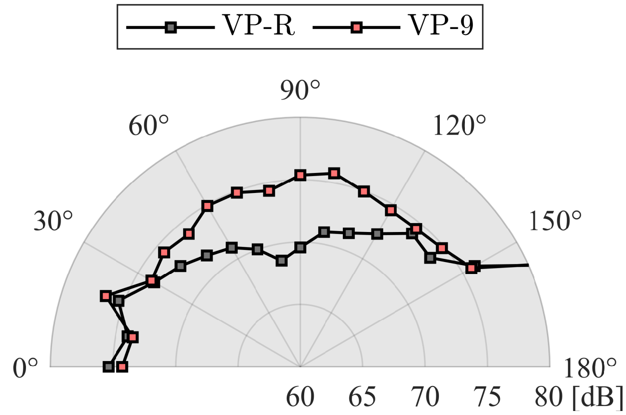

Figure 12: Directivity OASPL at 5000 RPM.

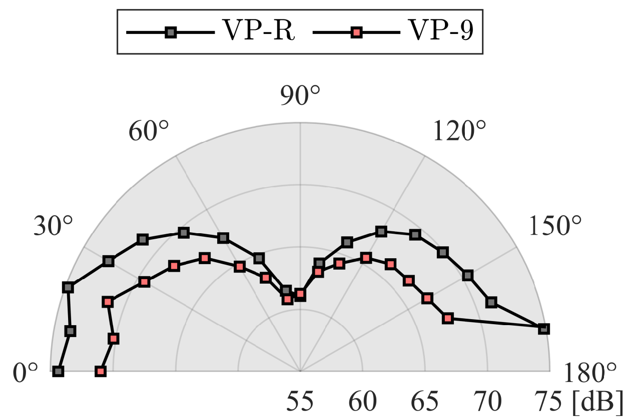

Figure 13: Directivity OASPLA at 5000 RPM.

CONCLUDING REMARKS

This study presented an experimental investigation into the aerodynamic and aeroacoustic performance of radially asymmetric, two-bladed propellers with a 90-degree blade spacing, under static flight conditions. Comparative analysis with a symmetric reference propeller revealed perceptually significant acoustic differences with minimal penalty in aerodynamic efficiency. Based on the analysis presented, the following concluding remarks are drawn:

1. Static performance tests demonstrated that the VP-9 propeller, with a 90-degree blade spacing, exhibited aerodynamic efficiency parity with the reference VP-R propeller in terms of Figure of Merit, while showing a slight reduction in both thrust and torque at any angular speed.
2. The analysis revealed an asymmetric downwash distribution between the leading and trailing blades of the VP-9 propeller. The leading blade experienced a reduced downwash compared to the VP-R configuration, whereas the trailing blade experienced a greater increase. This imbalance contributed to the observed net thrust and torque deficit.

3. The free-field acoustic measurements showed that the Sound Power Level response of VP-9 propeller exhibited a pronounced increase in tones at intermediate harmonics of the BPF over the entire frequency domain.

   In the low-frequency domain, tones at principal harmonics were generally reduced or remained unchanged. At 5,000 rpm, the dominant increase of 30 dB and a decrease of 11 dB, respectively, were observed at 0.5BPF and 1BPF. This spectral behaviour was qualitatively consistent over the tested RPM range, corroborating previous findings.

   In the mid-frequency domain, the VP-9 propeller showed a reduction in all tones, ranging from approximately 3 dB to 6 dB. Furthermore, the VP-9 propeller exhibited a consistent reduction in broadband noise across the mid-frequency interval. It was hypothesised that the reduction in broadband noise is associated with the trailing-edge broadband noise.

   In the high-frequency interval, the VP-9 propeller experienced an increase in broadband noise. Given the spectral domain, this is likely associated with the bluntness vortex shedding. However, future investigation is required to confirm this statement.

4. Directivity analysis revealed that the VP-9 propeller exhibited a higher unweighted OASPL over most of the observation domain, with a peak increase of approximately 6 dB at the emission angles near the plane of rotation. When A-weighting filter was applied, the VP-9 propeller demonstrated a more favourable acoustic response at all observation angles when compared to the reference propeller, with a maximum reduction of approximately 3.4 dB in the axial direction at 5,000 rpm. As RPM was reduced, the perceived acoustic benefit of VP-9 became less apparent.

The findings of this study highlight the potential of uneven blade spacing as an effective strategy for mitigating perceptual noise in UAS applications, without significant performance degradation. By isolating the effect of a single asymmetric blade pair, the present work confirms that spectral redistribution can be achieved independently of multi-blade-pair interactions. This marks a contribution, demonstrating that simple geometric modifications can lead to meaningful shifts in acoustic signatures without requiring complex rotor systems.

Several aspects remain unresolved and require further investigation. In particular, it is necessary to determine the mechanism by which the broadband noise characteristics are altered due to the reduced blade spacing and how this can inform design improvements. Specifically, it should be confirmed if, and to what extent, the trailing blade is operating in an increased inflow turbulence due to the wake from the leading blade and how this impacts the noise sources.

Furthermore, while A-weighted measurements suggest a reduction in perceived loudness, whether the acoustic signature induced by the VP-9 propeller reduces subjective annoyance remains an open question. A psychoacoustic evaluation will be required to assess the subjective perceptual impact of such propeller configurations.

Finally, it is important to emphasise that the present analysis is limited to the specific propeller configurations, blade geometries, and static operating conditions tested. Although the findings qualitatively align with prior research, they cannot yet be generalised. Caution should be exercised when extrapolating these findings to propellers of different scales, blade geometries, or operational conditions.

Author contact:
Dima Usov dmitrij.usov@manchester.ac.uk

ACKNOWLEDGMENTS

This research is funded by the U.K. Engineering and Physical Sciences Research Council (EPSRC) Grant EP/W010119/1 for the GAAPS (Greener Aviation with Advanced Propulsion Systems) project. The authors would like to acknowledge the University of Salford's Acoustics Research Centre for access to the Anechoic Chamber, as well as Antonio J. Torija and his colleagues Deepak Akiwate, and Carlos Ramos-Romero for their assistance with the experimental setup. Antonio J. Torija would like to acknowledge the funding provided by: the U.K. Engineering and Physical Sciences Research Council Grant Number EP/V031848/1 for the DroneNoise project; the Innovate U.K. Ref. 73692 for the InCEPTion (Integrated Flight Control, Energy Storage and Propulsion Technologies for Electric Aircraft) project. Deepak Akiwate gratefully acknowledges the financial support provided by the University Fellowship through the University of Salford Fellowship Program.

REFERENCES

1. Schäffer, B., Pieren, R., Heutschi, K., Wunderli, J. M., and Becker, S., "Drone Noise Emission Characteristics and Noise Effects on Humans—A Systematic Review," *International Journal of Environmental Research and Public Health*, Vol. 18, (11), 2021. DOI: 10.3390/ijerph18115940.
2. Torija, A. J., and Nicholls, R. K., "Investigation of Metrics for Assessing Human Response to Drone Noise," *International Journal of Environmental Research and Public Health*, Vol. 19, (6), 2022. DOI: 10.3390/ijerph19063152.
3. Civil Aviation Authority, "Noise measurements from eVTOL aircraft: A review of available data," , Mar 2023, https://www.caa.co.uk/our-work/publications/documents/content/cap2506/.
4. Federal Aviation Administration, "Advanced Air Mobility Implementation Plan," , Jul 2023, https://www.faa.gov/air-taxis/implementation-plan.
5. European Union Aviation Safety Agency, "Environmental Protection Technical Specifications applicable to VTOL-capable aircraft powered by non-tilting rotors," , Jul 2023, https://www.easa.europa.eu/en/document-library/product-certification-consultations/consultation-paper-environmental-protection.

6. Poggi, C., Rossetti, M., Bernardini, G., Iemma, U., Andolfi, C., Milano, C., and Gennaretti, M., "Surrogate models for predicting noise emission and aerodynamic performance of propellers," *Aerospace Science and Technology*, Vol. 125, 2022, pp. 107016. DOI: 10.1016/j.ast.2021.107016.
7. Abergo, L., Guardone, A., and Gori, G., "Towards a Two-Stage Multi-Fidelity Shape Optimization Approach to Noise Reduction in Urban Air Mobility Applications," AIAA Scitech 2025 Forum, 2025. DOI: 10.2514/6.2025-0245.
8. Poggi, C., Bernardini, G., Gennaretti, M., and Camussi, R., "Scalability of Mach Number Effects on Noise Emitted by Side-by-Side Propellers," *Applied Sciences*, Vol. 12, (19), 2022, pp. 9507.
9. Azuma, A., and Yasuda, K., "Flight performance of rotary seeds," *Journal of Theoretical Biology*, Vol. 138, (1), 1989, pp. 23–53. DOI: 10.1016/S0022-5193(89)80176-6.
10. Lentink, D., Dickson, W. B., van Leeuwen, J. L., and Dickinson, M. H., "Leading-Edge Vortices Elevate Lift of Autorotating Plant Seeds," *Science*, Vol. 324, (5933), 2009, pp. 1438–1440. DOI: 10.1126/science.1174196.
11. Mellin, R. C., and Sovran, G., "Controlling the Tonal Characteristics of the Aerodynamic Noise Generated by Fan Rotors," *Journal of Basic Engineering*, Vol. 92, (1), 03 1970, pp. 143–154. DOI: 10.1115/1.3424923.
12. Ewald, D., Pavlovic, A., and Bollinger, J. G., "Noise reduction by applying modulation principles," *Journal of the Acoustical Society of America*, Vol. 49, (5A), 1971, pp. 1381–1385. DOI: 10.1121/1.1912513.
13. Boltezar, M., Mesaric, M., and Kuhelj, A., "The Influence of Uneven Blade Spacing on The SPL and Noise Spectra Radiated from Radial Fans," *Journal of Sound and Vibration*, Vol. 216, (4), 1998, pp. 697–711. DOI: 10.1006/jsvi.1998.1707.
14. Cattanei, A., Ghio, R., and Bongiovı‘, A., "Reduction of the tonal noise annoyance of axial flow fans by means of optimal blade spacing," *Applied Acoustics*, Vol. 68, 11 2007, pp. 1323–1345. DOI: 10.1016/j.apacoust.2006.07.012.
15. Shahady, P., Lyon, C., Schauer, J., Chopin, M., and Ewing, M., "The effects of modulated blade spacing on static rotor acoustics and performance," Aeroacoustics Conference, 1973. DOI: 10.2514/6.1973-1020.
16. Chirico, G., Barakos, G. N., and Bown, N., "Numerical aeroacoustic analysis of propeller designs," *The Aeronautical Journal*, Vol. 122, (1248), 2018, pp. 283–315. DOI: 10.1017/aer.2017.123.
17. Dobrzynski, W., "Propeller Noise Reduction by Means of Unsymmetrical Blade-spacing," *Journal of Sound and Vibration*, Vol. 163, (1), 1993, pp. 123–126. DOI: 10.1006/jsvi.1993.1152.
18. Usov, D., Koning, D., Chronis, T., Filippone, A., Akiwate, D., and Martinez, A. J. T., "Aerodynamics and Acoustics of Asymmetric Propellers With Uneven Blade Spacing," 30th AIAA/CEAS Aeroacoustics Conference, 6 2024. DOI: 10.2514/6.2024-3265.
19. Koning, D., Usov, D., Romero, C. R., and Filippone, A., "Flight Performance and Acoustics of Asymmetric Propellers with Uneven Blade Spacing," Quiet Drones 2024, 2024. DOI: 10.17866/rd.salford.27886224.v1.
20. Casagrande Hirono, F., Torija Martinez, A., and Elliott, A., "Optimization of a contra-rotating propeller rig for reduced psychoacoustic impact," INTER-NOISE and NOISE-CON Congress and Conference Proceedings, Vol. 265, 2023. DOI: 10.3397/IN_2022_0584.
21. Akiwate, D. C., Joseph, P., Parry, A., and Paruchuri, C., "On the balance between the tonal and broadband noise of isolated propellers," *International Journal of Aeroacoustics*, Vol. 23, (1-2), 2024, pp. 122–153. DOI: 10.1177/1475472X231225631.
22. Tinney, C. E., and Sirohi, J., "Multirotor Drone Noise at Static Thrust," *AIAA Journal*, Vol. 56, (7), 2018, pp. 2816–2826. DOI: 10.2514/1.J056827.
23. Stephenson, J. H., Weitsman, D., and Zawodny, N. S., "Effects of flow recirculation on unmanned aircraft system (UAS) acoustic measurements in closed anechoic chambers," *The Journal of the Acoustical Society of America*, Vol. 145, (3), 03 2019, pp. 1153–1155. DOI: 10.1121/1.5092213.
24. Weitsman, D., Stephenson, J. H., and Zawodny, N. S., "Effects of flow recirculation on acoustic and dynamic measurements of rotary-wing systems operating in closed anechoic chambers," *The Journal of the Acoustical Society of America*, Vol. 148, (3), 09 2020, pp. 1325–1336. DOI: 10.1121/10.0001901.
25. Gojon, R., Jardin, T., and Parisot-Dupuis, H., "Experimental investigation of low Reynolds number rotor noise," *The Journal of the Acoustical Society of America*, Vol. 149, (6), 06 2021, pp. 3813–3829. DOI: 10.1121/10.0005068.
26. Casalino, D., Romani, G., Pii, L. M., and Colombo, R., "Flow confinement effects on sUAS rotor noise," *Aerospace Science and Technology*, Vol. 143, 2023, pp. 108756. DOI: doi.org/10.1016/j.ast.2023.108756.
27. Deters, R. W., Krishnan, G. K. A., and Selig, M. S., "Reynolds Number Effects on the Performance of Small-Scale Propellers," 32nd AIAA Applied Aerodynamics Conference, 6 2014. DOI: 10.2514/6.2014-2151.
28. Dantsker, O. D., Caccamo, M., Deters, R. W., and Selig, M., "Performance testing of APC electric fixed-blade UAV propellers," AIAA Aviation Forum, 2022. DOI: 10.2514/6.2022-4020.
29. Peters, D. A., and He, C. J., "Finite state induced flow models. II - Three-dimensional rotor disk," *Journal of Aircraft*, Vol. 32, (2), 1995, pp. 323–333. DOI: 10.2514/3.46719.
30. Usov, D., Chronis, T., Ardelean, I.-C., and Filippone, A., "On minimum power flight formations of lifting propellers," *Aerospace Science and Technology*, Vol. 149, 2024, pp. 109150. DOI: 10.1016/j.ast.2024.109150.
31. Welch, P., "The use of fast Fourier transform for the estimation of power spectra: A method based on time averaging over short, modified periodograms," *IEEE Transactions on Audio and Electroacoustics*, Vol. 15, (2), 1967, pp. 70–73. DOI: 10.1109/TAU.1967.1161901.
32. Sinibaldi, G., and Marino, L., "Experimental analysis on the noise of propellers for small UAV," *Applied Acoustics*, Vol. 74, (1), 2013, pp. 79–88. DOI: doi.org/10.1016/j.apacoust.2012.06.011.
33. McKay, R. S., Kingan, M. J., Go, S. T., and Jung, R., "Experimental and analytical investigation of contra-rotating

multi-rotor UAV propeller noise," *Applied Acoustics*, Vol. 177, 2021, pp. 107850.
DOI: doi.org/10.1016/j.apacoust.2020.107850.

34. Casalino, D., Grande, E., Romani, G., Ragni, D., and Avallone, F., "Definition of a benchmark for low Reynolds number propeller aeroacoustics," *Aerospace Science and Technology*, Vol. 113, 2021, pp. 106707.
DOI: doi.org/10.1016/j.ast.2021.106707.

35. Rossignol, K. S., Yin, J., and Rottmann, L., "Investigation of small-scale rotor aeroacoustic in DLR's acoustic Wind Tunnel Braunschweig," *28th AIAA/CEAS Aeroacoustics Conference, 2022*, 2022. DOI: 10.2514/6.2022-2838.

36. Tinney, C. E., and Valdez, J. A., "Higher-Order Statistical Metrics for Characterizing Multirotor Acoustics," *AIAA Journal*, Vol. 62, (11), 2024, pp. 4431–4441.
DOI: 10.2514/1.J064032.

37. Iannotta, M., Visingardi, A., Quagliarella, D., De Gregorio, F., Barbarino, M., and Zanotti, A., "Improvement of a Free-Wake Model for the Aerodynamic and Aeroacoustic Analysis of a Small-Scale Two-Bladed Propeller in Hover," *Aerospace*, Vol. 12, (1), 2025. DOI: 10.3390/aerospace12010005.

38. Usov, D., Chronis, T., Filippone, A., and Bojdo, N., "Performance of Asymmetric Propellers Under Varying Blade Spacing," 49th European Rotorcraft Forum, 2023.

39. Botero-Bolívar, L., dos Santos, F. L., Venner, C. H., and de Santana, L., "Increase of Unsteady Pressure at a Trailing Edge due to Inflow Turbulence," *AIAA Journal*, Vol. 60, (12), 2022, pp. 6798–6813. DOI: 10.2514/1.J061670.

40. Botero-Bolívar, L., dos Santos, F. L., Venner, C. H., and de Santana, L., "Influence of the Freestream Turbulence on Wall-Pressure Fluctuations Along an Airfoil Chord," *AIAA Journal*, Vol. 61, (5), 2023, pp. 2309–2313.
DOI: 10.2514/1.J062567.

41. Zawodny, N. S., Boyd Jr, D. D., and Burley, C. L., "Acoustic Characterization and Prediction of Representative, Small-Scale Rotary-Wing Unmanned Aircraft System Components," American Helicopter Society (AHS) International Forum 72, 5 2016.
DOI: 10.4050/F-0072-2016-11346.

APPENDIX

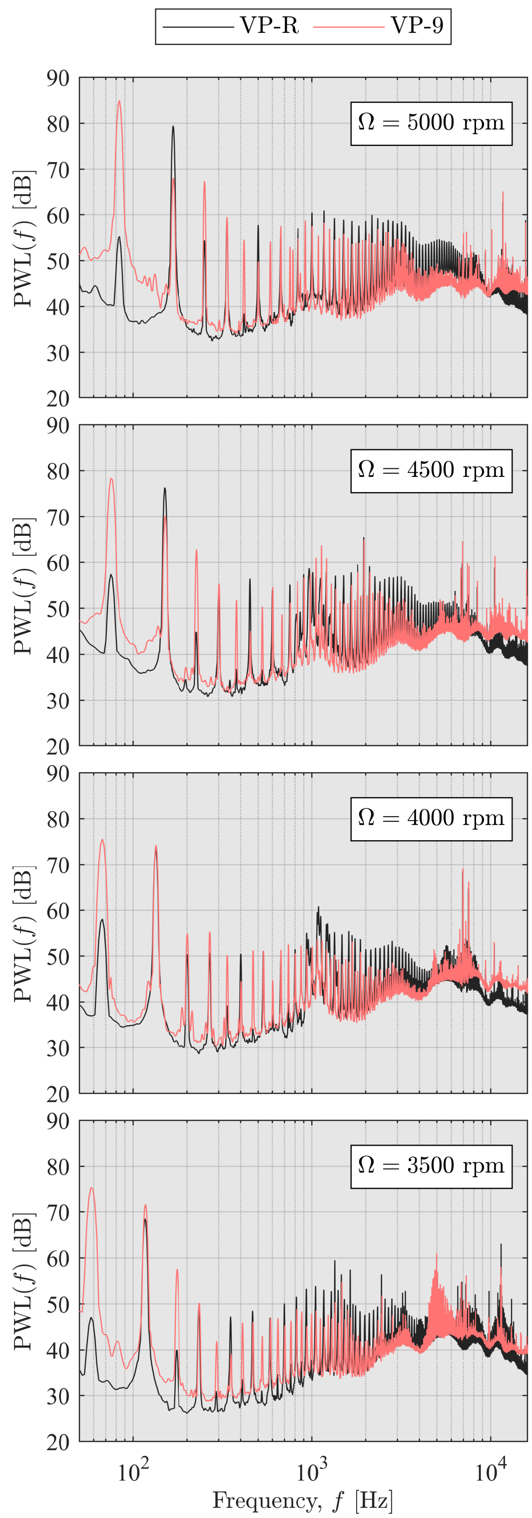

Figure 14: Sound Power Level.

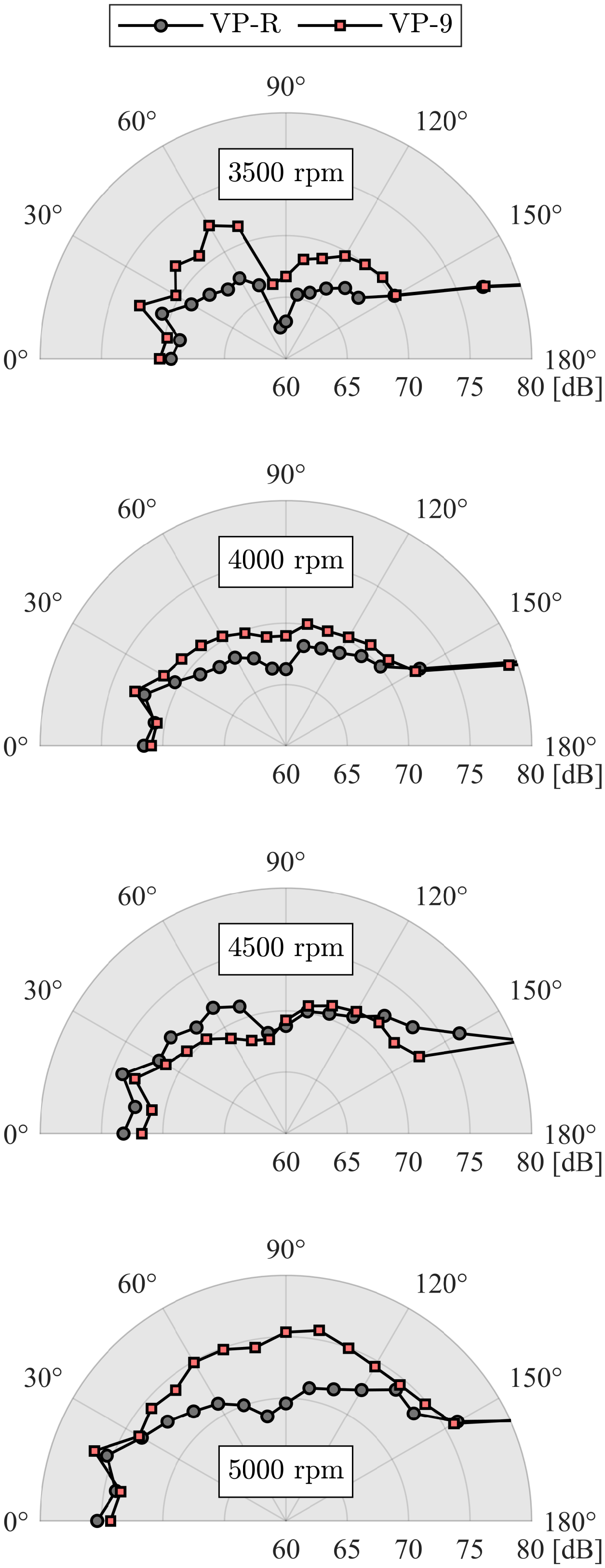

Figure 15: Directivity OASPL.

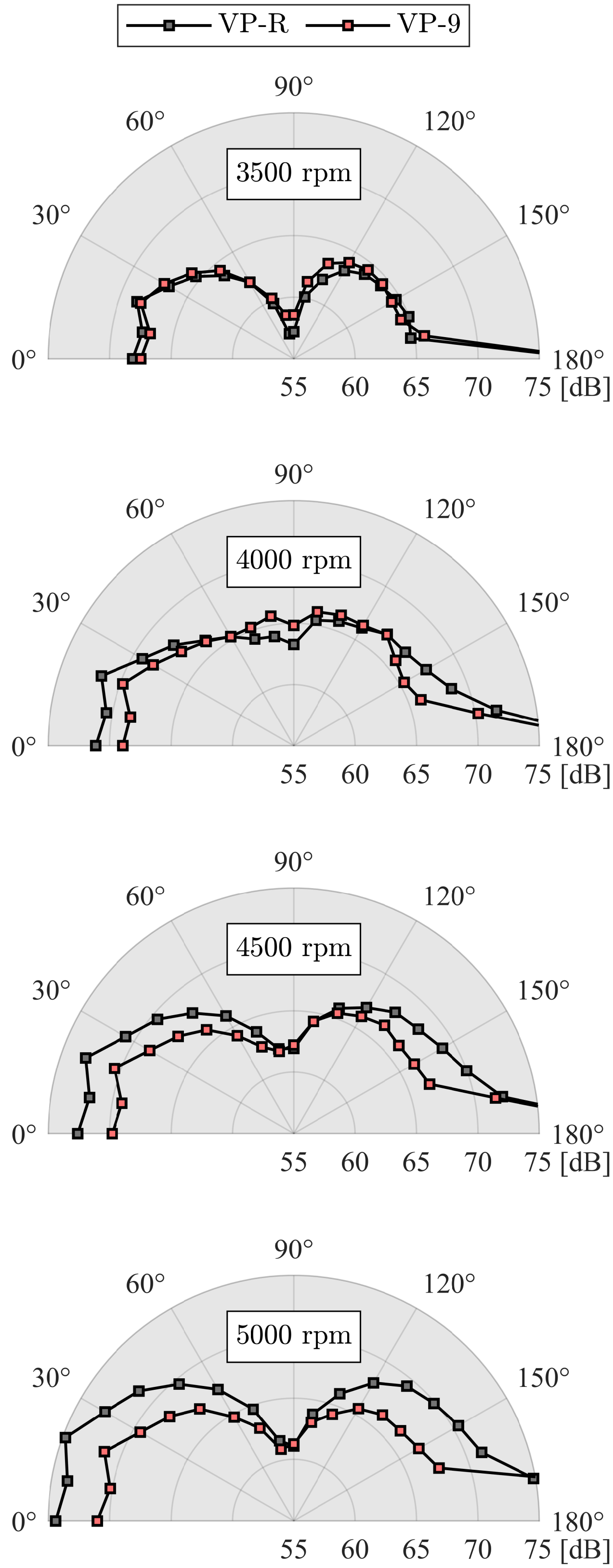

Figure 16: Directivity OASPLA.